Optical Generation of Hot Plasmonic Carriers in Metal Nanocrystals: The Effects of Shape and Field Enhancement

ARTICLE *in* THE JOURNAL OF PHYSICAL CHEMISTRY C · APRIL 2014

Impact Factor: 4.77 · DOI: 10.1021/jp500009k

2 AUTHORS:

Hui Zhang
Rice University
39 PUBLICATIONS **404** CITATIONS
SEE PROFILE

Alexander O Govorov
Ohio University
143 PUBLICATIONS **4,614** CITATIONS
SEE PROFILE

THE JOURNAL OF PHYSICAL CHEMISTRY C

Article

pubs.acs.org/JPCC

Optical Generation of Hot Plasmonic Carriers in Metal Nanocrystals: The Effects of Shape and Field Enhancement

Hui Zhang and Alexander O. Govorov*

Department of Physics and Astronomy, Ohio University, Athens, Ohio 45701, United States

Supporting Information

ABSTRACT: We investigate theoretically photogeneration of excited carriers in plasmonic nanocrystals. The theory is based on the solution of the quantum equation of motion for the density matrix. Efficient photogeneration of plasmonic electrons and holes in small nanocrystals becomes possible due to the nonconservation of the electron momentum. The confinement and reflection of electrons in small nanocrystals allowed photon-assisted electron transitions with high excitation energies and therefore lead to a large number of energetic carriers. This process is a surface-scattering effect and efficient only for nanostructures with small sizes. Other important factors for the photogeneration effect are the field enhancement and the inhomogeneity of electromagnetic fields inside a plasmonic nanostructure. The plasmonic field effects strongly depend on the shape of the nanocrystal. For example, a plasmonic nanocube is more efficient for the electron photogeneration than a nanosphere and a nanosphere generates more energetic carriers compared to a plasmonic slab. The results obtained here can be used for designing plasmonic nanostructures for solar and photocatalytic applications.

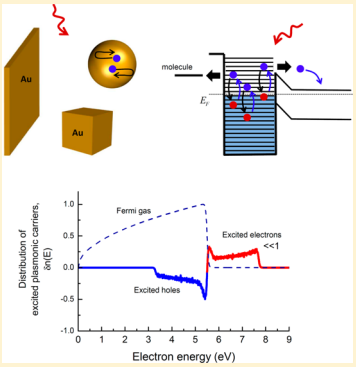

1. INTRODUCTION

Generation of hot plasmonic carriers is an active direction of research in the field of nanoplasmonics. This topic involves two types of potential and current applications. The first one is the photodetectors based on the Schottky junction[1] and the second one is related to the photocatalytic processes.[2−4] The advantage of plasmonic injectors is the large and resonant absorption cross sections of metal nanocrystals and nanoantennas. Over the last years a large number of experimental studies have been performed in this area involving both solid-state structures[5−13] for electronic photocurrents and colloidal solutions[14−25] for surface photochemistry. Theoretically, photoinjection of electrons in a semiconductor-metal Schottky-barrier device is described by the Fowler theory[26] that is based on the phenomenological assumption of isotropic and energy-independent generation of excited carriers. However, recent experiments with plasmonic nanoantennas suggested that excited-carrier distributions may have directionality in the momentum space.[27] Recent theoretical papers presented further developments of the Fowler theory involving reflection of electron waves in films[28,29] and effects of plasmonic fields.[30−32] Quantum theories for the internal and external photoelectric effects in bulk materials offer the equations for the photogenerated currents across the interface of two media.[33,34] These equations were recently employed for an evaluation of the photoinjection efficiency in plasmonic nanostructures.[35,36] Another recent theoretical paper treated a steady state of optically driven metal nanocrystals using an effective temperature approach and kinetic equations.[37]

Here, we study numerically the effect of the generation of hot plasmonic carriers in metal nanocrystals (NCs) with various shapes. Our approach is based on a solution for the density matrix and on the numerical evaluation of the electron distribution functions. In our previous study,[38] we have developed a semiquantitative analytical approach to this problem and applied it to the slab geometry. In this paper we present quantitative numerical solutions of the problem for NCs of various shapes. We show that the rate of generation of hot plasmonic carriers strongly depends on the shape of NC. Two physical reasons lead to the shape effects. First, the plasmonic field enhancement and the inhomogeneity of electric fields inside a NC, which amplify the generation of carriers, strongly depend on the shape. Second, the electron confinement in a NC is shape-dependent and, therefore, the photogeneration of energetic carriers, which is induced by the confinement, becomes shape-dependent as well. The electron confinement comes from the backscattering of electrons from the potential walls of NC. This scattering effect and the related nonconservation of momentum create large amplitudes for the optical transitions from the Fermi sea states to the highly excited levels in a NC. In fully confined geometries, the spectra of photogenerated electrons exhibit typically stronger oscillations as a function of the electron energy. Another important development compared to our previous study[38] is the numerical ensemble averaging for the hot-electron distribution functions. This averaging method mimics an ensemble of colloidal nanocrystals with a certain size dispersion suspended in a solution or adsorbed on a surface of an electrode. In

Received: January 1, 2014
Revised: February 20, 2014
Published: March 19, 2014

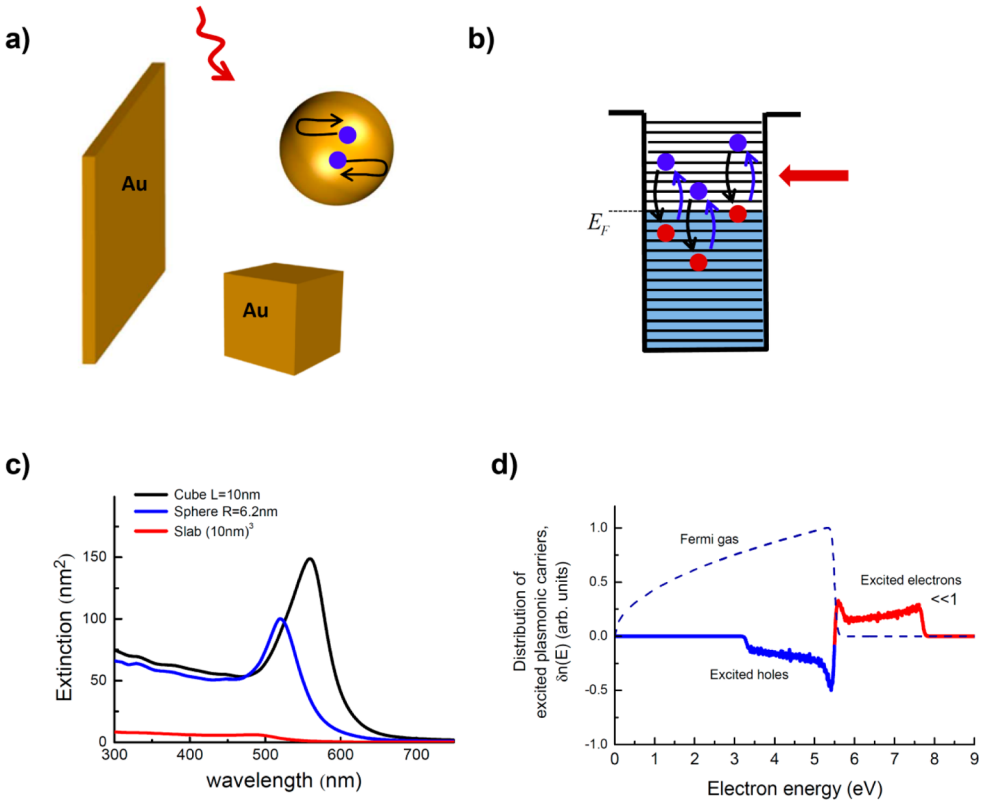

Figure 1. (a) Models of nanocrystals. (b) Illustration of excitation and relaxation processes in a nanocrystal with a Fermi sea of electrons. (c) Calculated extinctions of nanocrystals showing plasmon resonances. (d) Schematic illustration of the electron energy distribution in a photoexcited nanocrystal. The dashed curve shows the equilibrium Fermi distribution, whereas the colored solid curves give the excited electron and hole distributions.

addition, the size-averaging method removes fast oscillations of the electron distributions as a function of the optical energy and makes the quantitative analysis easier. In contrast to the other calculations[28−32,35−37] of the electron distributions in optically excited nanostructures, we derive the nonequilibrium electron population and the plasmonic wave function directly from the many-body density matrix. This allows us to obtain the microscopic description that is based on the optical matrix elements and the density of states in a NC. The study of plasmonic states presented here is based on the quantum equations and therefore has relevance to the subfield of plasmonics describing quantum[39−41] and nonlocal effects[42−44] in metal nanostructures. Our results should be useful for understanding plasmonic carrier generation that can be utilized in a variety of optoelectronic and photocatalytic systems.

2. FORMALISM AND MODELS

Metal nanocrystals (NCs) may have various shapes (Figure 1a). They absorb efficiently incident photons, which create electron−hole excitations in the Fermi gas (Figure 1b). To describe the dynamics of electrons in a NC, we will use the method of the equation of motion of the density matrix $\hat{\rho}$. The matrix elements of the density matrix obey the following equation:[45,46]

$$\hbar\frac{\partial\rho_{mn}}{\partial t} = i\langle m|[\hat{\rho}, \hat{H}_0 + \hat{V}_{\text{opt}}]|n\rangle - \Gamma(\hat{\rho}_{mn} - \hat{\rho}_{mn}^{(0)}) \quad (1)$$

where $\rho_{mn}^{(0)} = f_{\text{F}}(\varepsilon_n)\delta_{nm}$ is the equilibrium density matrix involving the Fermi distribution function; $\Gamma = \hbar/\tau$ is the relaxation rate; and correspondingly τ is the relaxation time.

The Hamiltonian in eq 1 contains two terms. The operator $\hat{H}_0$ is the single-particle Hamiltonian of NC and $\hat{V}_{\text{opt}}$ is the time-dependent light-matter interaction in the electron plasma:

$$\hat{V}_{\text{opt}} = V_a e^{-i\omega t} + V_b e^{i\omega t}$$

$$V_a = e\varphi_\omega(r), \quad V_b = e\varphi_\omega^*(r)$$

$$\varphi_\omega(r) = [\varphi_{0,\omega}(r) + \varphi_{\text{ind},\omega}(r)]$$

where $\varphi_{0,\omega}$ is the potential created by an incident monochromatic wave and $\varphi_{\text{ind},\omega}$ is the induced Coulomb potential in the plasma. This approach is equivalent to the so-called random-phase approximation method in the theory of many-body systems.[45] The physical meaning of the matrix elements is illustrated by this equation:

$$\rho_{mn}(t) = \langle\Psi(t)|\hat{c}_n^+\hat{c}_m|\Psi(t)\rangle$$

where $\hat{c}_n^+$ and $\hat{c}_m$ are the creation and annihilation operators, respectively, and $\Psi(t)$ is the time-dependent many-body wave function of the electron gas driven by the optical excitation. Using the perturbation theory, one can solve eq 1. We give the corresponding derivation in the Supporting Information. The diagonal elements of the density matrix determine the steady-state populations of electron states in a NC in the presence of external field. The general solution valid for any quantum system has the form:

dx.doi.org/10.1021/jp500009k | J. Phys. Chem. C 2014, 118, 7606−7614

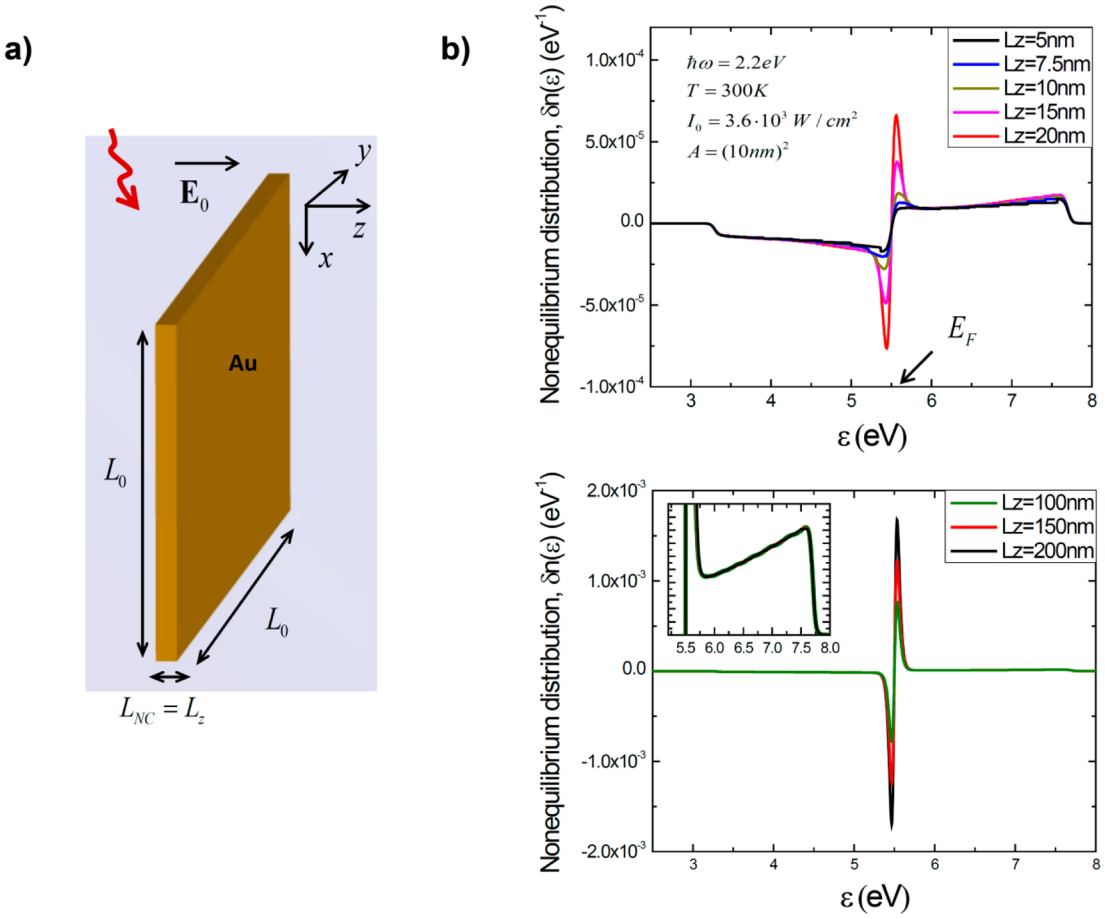

Figure 2. (a) Model of plasmonic platelet in water. The excitating electric field is perpendicular to the slab. (b) Calculated hot plasmonic electron distributions for slabs of different widths in the range of 5−150 nm. Inset: Blowup of the flat high-energy region of the distribution.

$$\rho_{nn} = \langle \Psi(t)|\hat{c}_n^+\hat{c}_n|\Psi(t)\rangle \approx f_F(E_n) + \delta\rho_{nn}^{(0)}$$

$$\delta\rho_{nn}^{(0)} = \frac{2}{\Gamma}\sum_{n'}(f_{n'} - f_n)\left[|V_{nn',a}|^2\frac{\Gamma}{(\hbar\omega - \varepsilon_n + \varepsilon_{n'})^2 + \Gamma^2} + |V_{nn',b}|^2\frac{\Gamma}{(\hbar\omega + \varepsilon_n - \varepsilon_{n'})^2 + \Gamma^2}\right] \quad (2)$$

where $f_n = f_F(\varepsilon_n)$ and

$$V_{nm,a} = \langle n|e\varphi_\omega(r)|m\rangle$$

Here $|m\rangle$ and ε_m are the single-particle states and their energies, correspondingly. In general, the elements ρ_{nn} may depend on time, but the main contribution to ρ_{nn} within the perturbation theory used here is time-independent (see the Supporting Information). The perturbation of the energy distribution function then can be constructed from eq 2 in the following way

$$\delta n(\varepsilon) = 2\sum_{\mathbf{n}}\delta\rho_{nn}\Phi(\varepsilon - \varepsilon_n) \quad (3)$$

where the coefficient 2 comes from the spins and $\Phi(\varepsilon - \varepsilon_n)$ plays the role of a delta function in the discrete sum.

$$\Phi(\varepsilon) = \frac{1}{\delta\varepsilon}, \quad |\varepsilon| < \delta\varepsilon/2$$

$$\Phi(\varepsilon) = 0, \quad |\varepsilon| > \delta\varepsilon/2$$

where $\delta\varepsilon$ should be taken small when computing the sum by eq 3. Then, the total distribution function of electrons in a NC under an optical excitation becomes

$$n(\varepsilon) = \frac{dN}{d\varepsilon} = n_F(\varepsilon) + \delta n(\varepsilon)$$

$$n_F(\varepsilon) = f_F(\varepsilon)\mathrm{DOS}(\varepsilon) \quad (4)$$

where $\mathrm{DOS}(E)$ is the density of states of a NC. Figure 1d illustrates the functions $n_F(E)$ and $\delta n(E)$.

In the following, we will apply eq 3 to Au NCs of various shapes with relatively small dimensions, about 5 nm. For such NCs, the size-quantization effects are very strong and accordingly lead to strong oscillations of the function $\delta n(\varepsilon,\omega)$. However, experiments are typically performed with large ensembles of metal NCs in a solvent. Such experiments do not usually show size-quantization effects in metal NCs. One of the reasons for this behavior is a dispersion of sizes of NCs in a large ensemble. To account for this effect, we need to perform an averaging over a size of NC. This averaging is absolutely necessary for a description of experiments with liquid solutions of NCs. A simple way to introduce a size-averaging is to perform the integration:

dx.doi.org/10.1021/jp500009k | J. Phys. Chem. C 2014, 118, 7606−7614

$$\delta\bar{n}(\varepsilon) = \frac{1}{\sqrt{\pi}\,\Delta}\int_{-\infty}^{+\infty} \mathrm{d}L e^{-[(L-L_0)/\Delta]^2}\delta n(\varepsilon, L) \quad (5)$$

where Δ is the parameter describing a dispersion of NC sizes. In eq 5, we use for simplicity the Gaussian distribution of sizes. The averaging eq 5 is also applied to the DOS function of a NC. After averaging, the density of states of a NC becomes close to the bulk function

$$\mathrm{DOS}_{\mathrm{bulk}}(E) = \frac{V_{\mathrm{NC}}}{2\pi^2}\left(\frac{2m_0}{\hbar^2}\right)^{3/2}\sqrt{\varepsilon}$$

where V_{NC} is the NC volume. The nonequilibrium population depends on the matrix element $V_{nm,a} = \langle n|e\varphi_\omega(r)|m\rangle$ that should be calculated by using the amplitude of the light-induced electric potential. For this, we will use numerical solutions of the Maxwell's equations for the models shown in Figure 1a. For numerical calculations, it is more convenient to express this matrix element in terms of the local electric field:

$$\varphi_{nn',a} = \langle n|\varphi_\omega(r)|n'\rangle = \frac{\hbar^2}{m(\varepsilon_{\mathbf{n}} - \varepsilon_{\mathbf{n}'})}\int \mathrm{d}V\psi_{\mathbf{n}}(\mathbf{E}_\omega\vec{\nabla}\psi_{\mathbf{n}'})$$

where $\mathbf{E}_\omega = -\vec{\nabla}\varphi_\omega$ is the total electric field inside a NC. Local electric fields and an optical extinction of NCs exhibit plasmon resonances, which depend on the shape of a NC (Figure 1c). Therefore, it is expected that the process of generation of plasmonic carriers is strongly shape-dependent. The field enhancement and the optical absorption rate for our model NCs can be calculated in the following ways. The rate of absorption of light by a NC is given by

$$Q_{\mathrm{NC}} = \langle\int_{V_{\mathrm{NC}}} \mathrm{d}V\mathbf{j}\mathbf{E}\rangle_{\mathrm{time}} = \mathrm{Im}(\varepsilon_{\mathrm{Au}})\frac{\omega}{2\pi}\int_{V_{\mathrm{NC}}}\mathrm{d}V\mathbf{E}_\omega\mathbf{E}_\omega^* \quad (6)$$

where $\mathbf{j}_\omega = i\omega(\varepsilon_{Au} - 1)/4\pi\mathbf{E}_\omega$ is the current in a NC and $\varepsilon_{\mathrm{Au}}$ is the metal dielectric constant. Correspondingly, the absorption cross section is given by

$$\sigma_{\mathrm{NC}}(\omega) = \frac{Q_{\mathrm{NC}}}{I_0}, \quad I_0 = \frac{c_0\sqrt{\varepsilon_0}}{2\pi}E_0^2$$

Here E_0 is the amplitude of the incident field. The plasmonic amplification effect in a NC is described by the averaged field-enhancement factor

$$P_{\mathrm{NC}}(\omega) = \int_{V_{\mathrm{NC}}}\frac{\vec{E}_\omega\vec{E}_\omega^*}{E_0^2}\,\mathrm{d}V \quad (7)$$

Both quantities σ_{NC} and P_{NC} will be useful to interpret the results of calculations. We now turn to the concrete examples of NCs.

3. PLASMONIC SLAB/PLATELET

We start with the simplest, slab geometry (Figure 2a). The external electric field is perpendicular to the slab, $\mathbf{E}_0\|\hat{\mathbf{z}}$. This slab model can also serve as a good approximation for colloidal platelets in a solution. The single-particle spectrum of a slab is given by

$$\varepsilon_{\mathbf{n}} = \frac{\hbar^2\pi^2(n_x^2 + n_y^2)}{2m_0L_0^2} + \frac{\hbar^2\pi^2 n_z^2}{2m_0L_z^2} \quad (8)$$

where L_z is the slab width and L_0 is the lateral dimension of a slab; the surface area of a slab is then defined as $A = L_0^2$. The quantum state of an electron is described by the numbers $\mathbf{n} = (n_x, n_y, n_z)$, where $n_\alpha = 1, 2, 3, \ldots$. The corresponding wave functions of electrons are

$$\psi_{\mathbf{n}} = \sqrt{\frac{2^3}{L_0^2L_z}}\sin[k_{n_x}x]\sin[k_{n_y}y]\sin[k_{n_z}z]$$

$$\mathbf{k}_{\mathbf{n}} = (k_{n_x}, k_{n_y}, k_{n_y}) = \left(\frac{\pi}{L_0}n_x, \frac{\pi}{L_0}n_y, \frac{\pi}{L_z}n_z\right)$$

The electric field inside a slab is given by the boundary conditions and has the form:

$$E_\omega = \gamma_{\mathrm{slab}}(\omega)E_0, \quad \gamma_{\mathrm{slab}}(\omega) = \frac{\varepsilon_0}{\varepsilon_{\mathrm{Au}}}$$

where $\varepsilon_0 = 1.8$ is the dielectric constant of the matrix (water). The dielectric constant of gold is taken from ref 47. Then, the matrix elements of transitions are obtained in the following analytical form:

$$|V_{\mathbf{nn}',a}|^2 = \delta_{n_x,n_{x'}}\delta_{n_y,n_{y'}}(eE_0\gamma_{\mathrm{slab}}(\omega))^2\left(\frac{2L_z}{\pi^2}\right)^2 \left(\frac{1}{(n_z' - n_z)^2} - \frac{1}{(n_z' + n_z)^2}\right)^2$$

In the slab geometry, the equation for the electron distribution (eq 3) can be integrated over the in-plane quantum numbers (in-plane momenta) and the resulting equation becomes

$$\delta n(\varepsilon) = \frac{e^2}{\Gamma}A\frac{2}{\pi}\frac{m_0}{\hbar^2}\sum_{\substack{n'\geq 1\\ n\leq n_{\mathrm{crit}}(\varepsilon)}}\left(\frac{1}{e^{(\varepsilon-\varepsilon_{n_z}+\varepsilon_{n_z'}-\mu)/KT}+1} - \frac{1}{e^{(\varepsilon-\mu)/KT}+1}\right)|V_{n_zn_z',a}|^2 \left[\frac{\Gamma}{(\hbar\omega - \varepsilon_{n_z} + \varepsilon_{n_z'})^2 + \Gamma^2} + \frac{\Gamma}{(\hbar\omega + \varepsilon_{n_z} - \varepsilon_{n_z'})^2 + \Gamma^2}\right] \quad (9)$$

where

$$\varepsilon_{n_z} = \frac{E_L n_z^2}{2}, \quad E_L = \frac{\hbar^2\pi^2}{m_0L_z^2},$$

$$V_{n_zn_z',a} = \langle n_z|e\varphi_\omega(z)|n_z'\rangle, \; n_{\mathrm{crit}}(\varepsilon) = \sqrt{\frac{2m_0L_z^2}{\hbar^2\pi^2}\varepsilon}$$

The Fermi energy in this equation should be taken as $E_F = \mu = 5.5$ eV (gold). The corresponding Fermi velocity is $v_F = 1.4 \times 10^8$ cm/s. The decay parameter Γ describes the energy relaxation in gold and can be taken from the time-resolved experiments,[48,49] $\Gamma = \hbar/(0.5\ \mathrm{ps}) = 0.0013$ eV. Figures 2–4 present the calculations for the Au slab in water. For averaging we used the parameter $\Delta = 1$ nm.

The plasmonic electron distributions have a positive region at $\varepsilon > E_F$ and a negative region below the Fermi level (Figure 2b). These regions describe optical generation of electrons and holes in the Fermi sea. As described earlier in ref 38, for small NCs, the plasmonic-carrier distribution is nearly flat for the

dx.doi.org/10.1021/jp500009k | J. Phys. Chem. C 2014, 118, 7606−7614

electron and hole intervals. For large NCs, the distribution function exhibits strong peaks at the Fermi energy and the flat regions of the distribution have less weight. In the 3D case, the nonequilibrium electron distribution in a plasmonic wave has only the peaks in the vicinity of the Fermi energy.[38] The flat regions of the distribution are surface effects and do not depend on the width of the slab. Excited carriers in the flat regions originate from the optical absorption assisted by the scattering of electrons off the potential walls of a slab. In our quantum theory such backscattering effects are built into the wave functions. From the analytical theory,[38] we can write an approximated expression for the electron population in the flat regions

$$\delta n \approx \frac{(\hbar k_L v_F)^4}{\pi^2(\hbar\omega)^4}\frac{1}{\pi^2}\frac{|eL_z\gamma_{slab}E_{\omega,0}|^2}{\Gamma E_L{}^2}\left(\frac{V_{NC}}{L_z{}^3}\right) \approx AL_z{}^0\frac{|\gamma_{slab}(\omega)|^2}{\omega^4} \tag{10}$$

where the key parameter is

$$k_L = \frac{\pi}{L_z}$$

The momentum k_L determines the transfer of momentum to an excited electron in the process of optical absorption. In a slab or a NC, the linear momentum is not conserved and this gives the possibility to excite electrons and holes with high energies $\varepsilon \approx E_F \pm \hbar\omega$. The flat regions in the energy distribution (Figure 2b) appear due to the transitions $n' \to n$ with large changes $|\Delta n_z| = |n_z - n_{z'}| \gg 1$. Such transitions conserve the energy $\varepsilon_{n_z} - \varepsilon_{n_{z'}} \approx \hbar v_F k_L \Delta n_z \approx \hbar\omega$. In the Supporting Information, we give an illustration for the Fermi sea and the important transitions with $\varepsilon_{n_z} - \varepsilon_{n_{z'}} \approx \hbar\omega$. Such transitions are responsible for photogeneration of energetic carriers in a NC. The characteristic change of the electron quantum number for these transitions is then given by $\Delta n_z \approx \hbar\omega/\hbar v_F k_L \gg 1$. The flat regions of the function $\delta n(\varepsilon)$ in Figure 2b extend over the whole interval $E_F - \hbar\omega < \varepsilon < E_F + \hbar\omega$. The peaks at the Fermi level (Figure 2b) have a different origin. Their width is about $3k_BT + \hbar v_F k_L$ and they come from the transitions $n' \to n \pm 1$ in the sum eq 9. These peaks at the Fermi level (Figure 2b) represent a bulk effect and, for a large width of NC, the peak amplitudes are proportional to the NC volume, i.e. $\delta n_{peak} \approx AL_z$. With increasing L_z the picture evolves from the strongly confined case to the 3D regime of the bulk plasmon wave. For small L_z, the flat regions dominate the picture and the slab has a large fraction of highly excited electrons (holes), whereas for large L_z, the majority of nonequilibrium carriers have small excitation energies and are found in the interval $E_F - 3k_BT < \varepsilon < E_F + 3k_BT$. More calculations describing this behavior can be found in the Supporting Information.

It is interesting to compare the plasmonic generation effect with the other optical properties of a slab. Figure 3 shows simultaneously the extinction, the field enhancement, and the hot-carrier population. We see that these properties exhibit different spectral shapes. To some extent, the population of excited electrons resembles the field-enhancement factor $P = |\gamma_{slab}(\omega)|^2$. This can be understood from the analytical eq 10, which tells that $\delta n \approx |\gamma_{slab}(\omega)|^2/\omega^4$. Simultaneously, the extinction and the hot-electron population can be significantly different, especially for large photon energies (Figure 3). The reason is in the interband transitions. The generation of plasmonic carriers considered here comes from the intraband

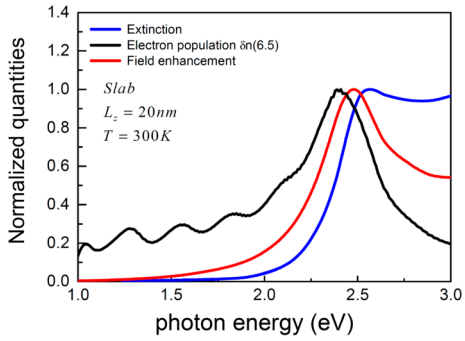

Figure 3. Comparison between the optical characteristics of a slab. The graph depicts simultaneously the extinction, the field enhancement, and the hot-carrier population of a 10-nm Au slab in water.

transitions, whereas the extinction calculated with the empirical dielectric function also includes a large contribution from the interband processes.[38]

As we mentioned above, the population of energetic carriers is important for understanding photocatalytic reactions on the surface of plasmonic nanocrystals. In photochemical reactions, it is important to know the number of excited electrons with the energy equal to the energies of reacting molecules. Figure 4 illustrates this case. A molecule can be reduced by accepting a photoexcited electron from a NC or oxidized by transferring an electron to a NC. The rates of the transfer processes are proportional to the nonequilibrium populations of carriers in a NC at the corresponding energies:

$$\text{rate}_{\text{reduction}} \propto \delta n(\varepsilon = E_F + \Delta E_{\text{mol},e})$$

$$\text{rate}_{\text{oxidation}} \propto 1 - \delta n(\varepsilon = E_F - \Delta E_{\text{mol},h})$$

In Figure 4, we show the calculated populations of a 20-nm slab as a function of the photon energy. Since we involve here highly excited carriers with energies $E - E_F \gg \hbar v_F(\pi/L_z)$ and $E - E_F \ll \hbar v_F(\pi/L_z)$, the frequency dependences for the populations can be approximated as:

$$\delta n(\omega, E = E_F + \Delta E_{\text{mol}}) \propto \frac{|\gamma_{slab}(\omega)|^2}{\omega^4}$$

$$1 - \delta n(\omega, E = E_F - \Delta E_{\text{mol}}) \propto \frac{|\gamma_{slab}(\omega)|^2}{\omega^4} \tag{11}$$

These functions reflect the plasmon resonance in a slab via the resonant factor $\gamma_{slab}(\omega) = \varepsilon_0/\varepsilon_{Au}(\omega)$. Another important factor in eq 11 is the multiplier ω^{-4} that comes from the quantum-mechanical optical matrix elements and the density of states in a NC. In the Supporting Information one can find a short description of another application of plasmonic carriers that is the photoinjection into a Schottky barrier.

4. CONFINED NANOCRYSTALS: SPHERE AND CUBE

We now consider the effect of plasmonic electron generation in NCs of different shapes. The general formalism develops in the same way and is based on eqs 2 and 3 that can be rewritten as

dx.doi.org/10.1021/jp500009k | J. Phys. Chem. C 2014, 118, 7606−7614

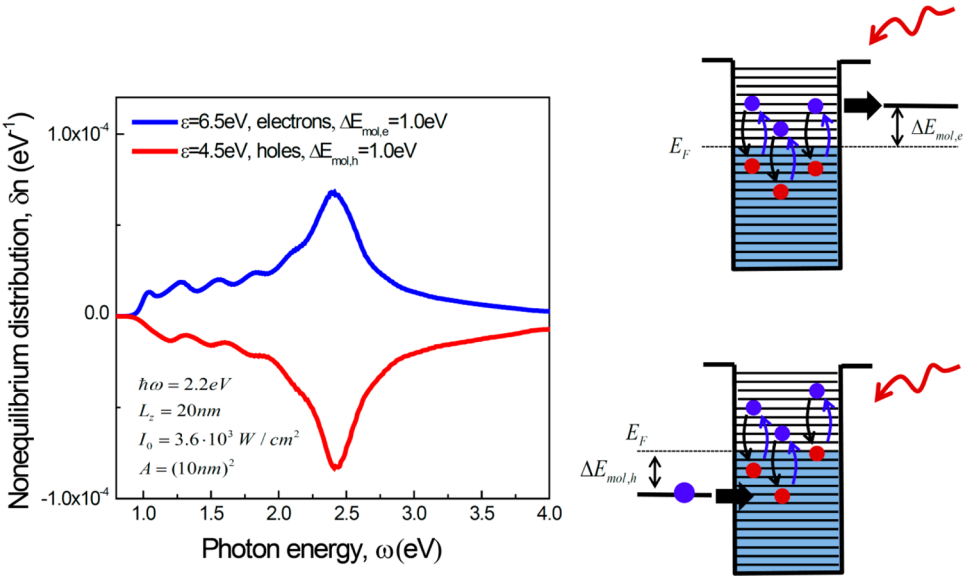

Figure 4. Calculated populations of a 20-nm slab as a function of the photon frequency for two particular electronic energies $E = E_F \pm 1$ eV. Insets: Energy diagrams of photoexcited NCs interacting with adsorbed molecules.

$$\delta n(\varepsilon) = \frac{4}{\Gamma}\sum_{\mathbf{n},\mathbf{n}'}\Phi(\varepsilon - \varepsilon_{\mathbf{n}})(f_{\mathbf{n}'} - f_{\mathbf{n}})\left[|V_{\mathbf{n}\mathbf{n}',a}|^2\frac{\Gamma}{(\hbar\omega - \varepsilon_{\mathbf{n}} + \varepsilon_{\mathbf{n}'})^2 + \Gamma^2} + |V_{\mathbf{n}\mathbf{n}',b}|^2\frac{\Gamma}{(\hbar\omega + \varepsilon_{\mathbf{n}} - \varepsilon_{\mathbf{n}'})^2 + \Gamma^2}\right]$$

Importantly, the single-electron energies and wave functions depend on the type of NC. For a sphere with infinite potential walls, the single-electron energies and wave functions have the following form:[50]

$$\varepsilon_{\mathbf{n}} = \varepsilon_{n,l,m}, \quad \psi_{\mathbf{n}} = e^{im\varphi}Y_{lm}(\varphi, \theta)u_{nl}(r)$$

where we used the spherical coordinates. The energies $\varepsilon_{n,l,m}$ should be found from the boundary conditions at the infinite potential walls. For the case of a cube, the electron spectrum is given by eq 8.

Inside a plasmonic sphere, the electric field is given by a simple analytical equation:

$$E_\omega = \gamma_{\text{sphere}}(\omega)E_0, \quad \gamma_{\text{sphere}}(\omega) = \frac{3\varepsilon_0}{\varepsilon_{\text{Au}} + 2\varepsilon_0}$$

In the case of a plasmonic cube, we need to use a numerical solution for the electric field $\mathbf{E}_\omega$. For this we employ the Discrete Dipole Approximation (DDA).[51−55] A plasmonic cube has enhanced electric fields at the vertices. In our numerical calculations, we round the vertices of a cube using nonzero radii and then evaluate the matrix elements $\varphi_{\mathbf{n}\mathbf{n}',a}$. For small radii of rounding, the optical matrix elements do not depend on the rounding radius and converge well. Therefore, the numerical procedure is reliable.

Figures 5 and 6 show the numerical results for three types of NCs. In particular Figure 6 gives the field-enhancement factor and the total numbers of excited electrons (holes):

$$\delta n_{\text{electrons,tot}} = \delta n_{\text{holes,tot}} = \int_{E_F}^{\infty} d\varepsilon \delta n(\varepsilon) = -\int_0^{E_F} d\varepsilon \delta n(\varepsilon)$$

The calculated NCs (slab, sphere, and cube) have the same volume (5 nm^3). In the case of the slab, we take the width 5 nm and the effective area of 5 nm^2. We observe the following: (1) The sphere and the cube exhibit strong oscillations of the distribution function due to the optical transitions between single-particle levels in the Fermi gas, whereas the slab case does not have strong oscillations. (2) The fully confined NCs (sphere and cube) have strongly enhanced rates of generation of plasmonic carriers when compared to the slab case. The strong oscillations of the electron distributions in the cases of sphere and cube come from the fully quantized character of the electronic spectrum in a NC (Figure 5). In the slab case, the quantization is applied only to the z-motion and the electron distribution function shows only small steps (Figure 5). Regarding the magnitudes of the hot-electron generations, the physical reason is less obvious. Qualitatively, since the hot-electron generation involves the transition matrix elements $\int d\mathbf{V}\psi_{\mathbf{n}}(\mathbf{E}_\omega\vec{\nabla}\psi_{\mathbf{n}'})$, the function $\delta n(\varepsilon)$ should be proportional to the field enhancement factor $P(\omega)$. However, interestingly, this physical argument is not sufficient to explain fully the strong increase of generation in the cubic NCs (Figure 6). The plasmonic field-enhancement factor increases when we move from the slab case to the spherical NP and then to the cube (Figure 6a). However, the increase of the field enhancement factor from the slab to the cube is 150-fold. Simultaneously, the increase of the total number of excited electrons in the cube is larger than the 150-fold amplification due to the electromagnetic enhancement. We interpret this result in terms of increased amplitudes of transitions with large excitation energies because the electromagnetic fields become strongly enhanced and nonuniform in the cubic geometry. Such strongly enhanced and inhomogeneous fields appear in the vicinity of the vertexes of plasmonic cube and produce significant matrix elements $\int d\mathbf{V}\psi_{\mathbf{n}}(\mathbf{E}_\omega\vec{\nabla}\psi_{\mathbf{n}'})$ between the pairs of electronic states $\psi_{\mathbf{n}}$ and $\psi_{\mathbf{n}'}$ with well separated energies. Our numerical calculations clearly show the appearance of significant quantum amplitudes for such transitions to highly excited states. However, when we move from the slab geometry to the spherical nanoparticle, the calculated increase in the electron photogeneration is not as strong since the electromagnetic field

dx.doi.org/10.1021/jp500009k | J. Phys. Chem. C 2014, 118, 7606−7614

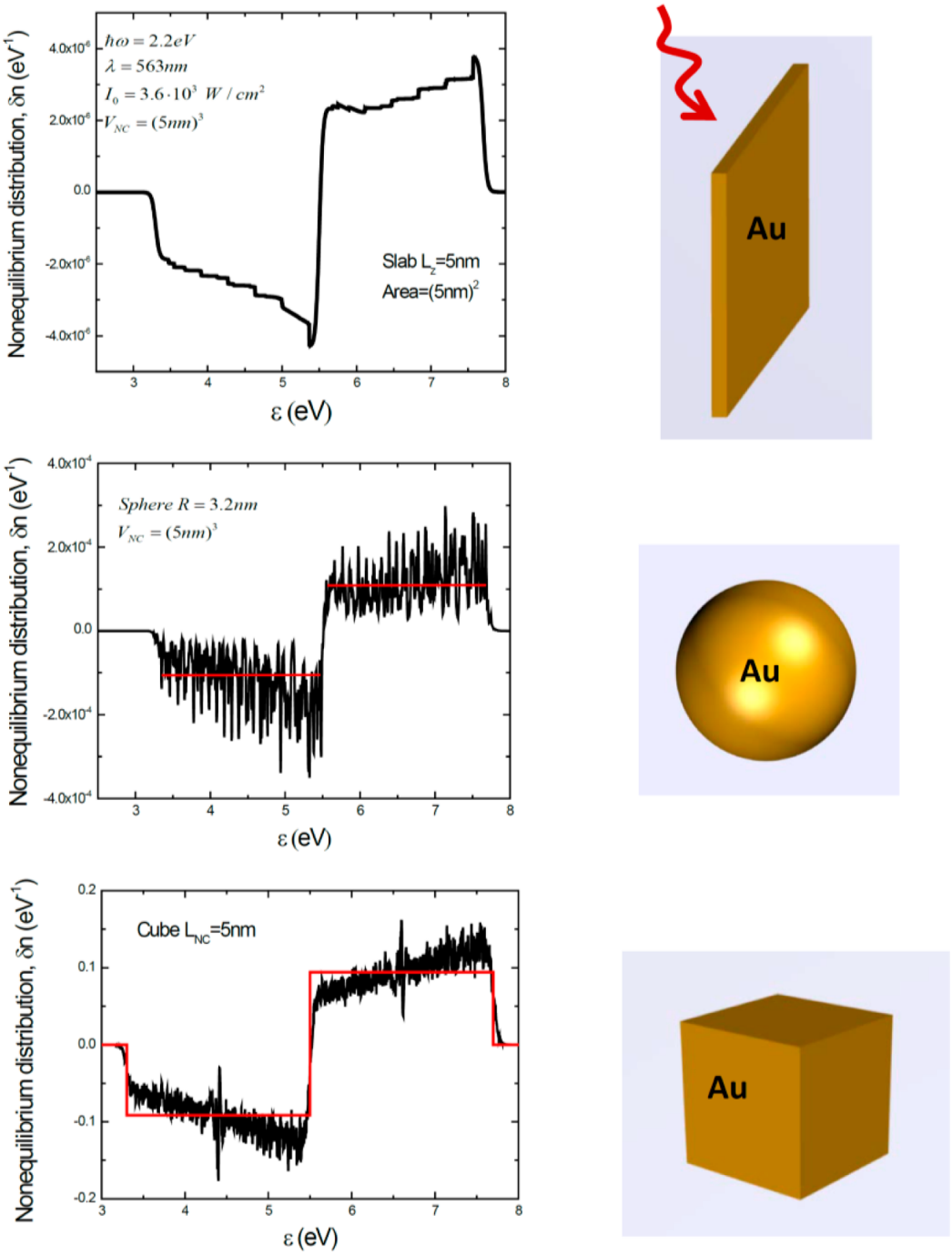

Figure 5. Calculated plasmonic electron distributions for a slab, a sphere, and a cube. The averaging parameter was Δ = 1 meV and the volumes of the NCs were kept the same. The red lines show the averaged values for the electron populations. The insets give the geometrical models.

in a small spherical NC is uniform and this field does not create excited states with high energies so efficiently. The calculated increase in the photogeneration for a spherical NC, compared to the slab case, comes mostly from the increased electromagnetic fields (Figure 6b). To summarize, in an ideal bulk system without defects and phonon scattering, the generation of highly excited electrons with energies $\sim\hbar\omega$ is impossible due to the conservation of momentum. In the case of NCs, the linear momentum is not conserved due to the confinement effect and the plasmonic inhomogeneous fields. Therefore, the generation of high-energy electrons and holes becomes possible in nanostructures and this process is efficient in nanocrystals with small dimensions.

5. CONCLUSIONS

We have studied the effect of photogeneration of excited carriers in plasmonic NCs of various shapes and sizes. The details of the electronic structure and the shapes of NCs are very important for the description of the effect of plasmonic electrons. In NCs, the generation of highly excited electrons is a surface effect and appears due to the nonconservation of the electron momentum. In fully confined NCs, such as plasmonic spheres and cubes, the effects of confinement are much

dx.doi.org/10.1021/jp500009k | J. Phys. Chem. C 2014, 118, 7606−7614

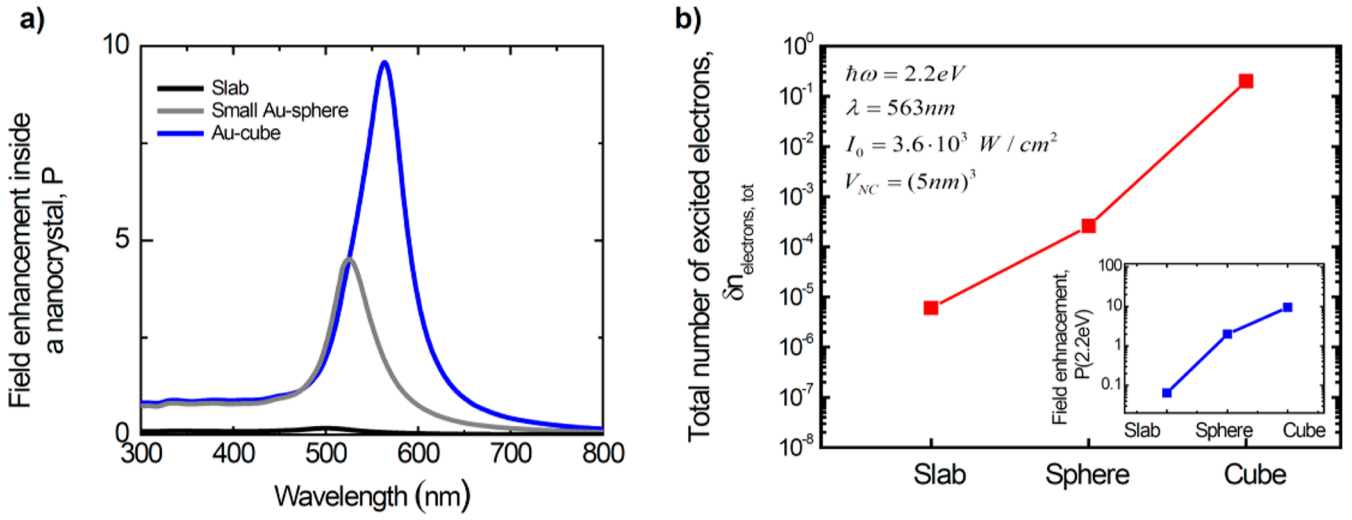

Figure 6. (a) Plasmonic field-enhancement factors for the three types of nanocrystals. (b) Calculated total number of photoexcited electrons for the nanocrystals at ω = 2.2 eV. Inset: Calculated field-enhancement factors at ω = 2.2 eV.

stronger, resulting in strong oscillations of the spectra of photogenerated electrons. A strong shape dependence of photogeneration also comes from the plasmonic field enhancement factor and the inhomogeneous fields in a NC. These effects are the strongest in the plasmonic nanocubes.

■ ASSOCIATED CONTENT

Supporting Information

Derivation for the time-dependent perturbation theory, energy diagram of transitions, and spectra of photogeneration of plasmonic electrons. This material is available free of charge via the Internet at http://pubs.acs.org.

■ AUTHOR INFORMATION

Corresponding Author

*E-mail: Govorov@ohiou.edu.

Notes

The authors declare no competing financial interest.

■ ACKNOWLEDGMENTS

This work was supported by the NSF (project: CBET-0933782) and the Volkswagen Foundation.

■ REFERENCES

(1) Sze, S. M.; Ng, K. K. *Physics of Semiconductor Devices*, 3rd ed.; Wiley: Hoboken, NJ, 2007.
(2) Frischkorn, C.; Wolf, M. Femtochemistry at Metal Surfaces: Nonadiabatic Reaction Dynamics. *Chem. Rev.* **2006**, *106*, 4207−4233.
(3) Linic, S.; Christopher, P.; Ingram, D. B. Plasmonic-Metal Nanostructures for Efficient Conversion of Solar to Chemical Energy. *Nat. Nanotechnol.* **2011**, *10*, 911−921.
(4) Kale, M. J.; Avanesian, T.; Christopher, P. Direct Photocatalysis by Plasmonic Nanostructures. *ACS Catal.* **2014**, *4*, 116−128.
(5) Mangold, M. A.; Weiss, C.; Calame, M.; Holleitner, A. W. Surface Plasmon Enhanced Photoconductance of Gold Nanoparticle Arrays with Incorporated Alkane Linkers. *Appl. Phys. Lett.* **2009**, *94*, 161104, 1−3.
(6) Knight, M. W.; Sobhani, H.; Nordlander, P.; Halas, N. J. Photodetection with Active Optical Antennas. *Science* **2011**, *332*, 702−704.
(7) Akbari, A.; Tait, R. N.; Berini, P. Surface Plasmon Waveguide Schottky Detector. *Opt. Express* **2010**, *18*, 8505−8514.
(8) Lee, Y. K.; Jung, C. H.; Park, J.; Seo, H.; Somorjai, G. A.; Park, J. Y. Surface Plasmon-Driven Hot Electron Flow Probed with Metal-Semiconductor Nanodiodes. *Nano Lett.* **2011**, *11*, 4251−4255.
(9) Conklin, D.; Nanayakkara, S.; Park, T.-H.; Lagadec, M. F.; Stecher, J. T.; Chen, X.; Therien, M. J.; Bonnell, D. A. Exploiting Plasmon-Induced Hot Electrons in Molecular Electronic Devices. *ACS Nano* **2013**, *7*, 4479−4486.
(10) Goykhman, I.; Desiatov, B.; Khurgin, J.; Shappir, J.; Levy, U. Locally Oxidized Silicon Surface-Plasmon Schottky Detector for Telecom Regime. *Nano Lett.* **2011**, *11*, 2219−2224.
(11) Casalino, M. Near-Infrared Sub-Bandgap All-Silicon Photodetectors: A Review. *Int. J. Opt. Appl.* **2012**, *2*, 1−16.
(12) Yan, F.; Sun, X. W. A Plasmonically Enhanced Charge Generation Layer for Tandem Organic Light Emitting Device. *Appl. Phys. Lett.* **2013**, *102*, 043303.
(13) Schuck, P. J. Nanoimaging: Hot electrons go through the barrier. *Nat. Nanotechnol.* **2013**, *8*, 799−800.
(14) Brus, L. Noble Metal Nanocrystals: Plasmon Electron Transfer Photochemistry and Single Molecule Raman Spectroscopy. *Acc. Chem. Res.* **2008**, *41*, 1742−1749.
(15) Wu, X.; Thrall, E. S.; Liu, H.; Steigerwald, M.; Brus, L. Plasmon Induced Plotovoltage and Charge Separation in Citrate-Stabilized Gold Nanoparticles. *J. Phys. Chem. C* **2010**, *114*, 12896−12899.
(16) Mubeen, S.; Lee, J.; Singh, N.; Krämer, S.; Stucky, G. D.; Moskovits, M. An Autonomous Photosynthetic Device in Which All Charge Carriers Derive from Surface Plasmons. *Nat. Nanotechnol.* **2013**, *8*, 247−251.
(17) Huschka, R.; Zuloaga, J.; Knight, M. W.; Brown, L. V.; Nordlander, P.; Halas, N. J. Light-Induced Release of DNA from Gold Nanoparticles: Nanoshells and Nanorods. *J. Am. Chem. Soc.* **2011**, *133*, 12247−12255.
(18) Xiao, M.; Jiang, R.; Wang, R.; Fang, C.; Wang, J.; Yu, J. C. Plasmon-enhanced Chemical Reactions. *J. Mater. Chem.* **2012**, *22*, 5790−5805.
(19) Mukherjee, S.; Libisch, F.; Large, N.; Neuman, O.; Brown, L. V.; Cheng, J.; Lassiter, J. B.; Carter, E. A.; Nordlander, P.; Halas, N. J. Hot Electrons do the Impossible: Plasmon-induced Dissociation of H_2 on Au. *Nano Lett.* **2013**, *13*, 240−247.
(20) Thomann, I.; Pinaud, B. A.; Chen, Z.; Clemens, B. M.; Jaramillo, T. F.; Brongersma, M. L. Plasmon Enhanced Solar-to-Fuel Energy Conversion. *Nano Lett.* **2011**, *11*, 3440−3446.
(21) Tong, H.; Ouyang, S.; Bi, Y.; Umezawa, N.; Oshikiri, M.; Ye, J. Nano-photocatalytic Materials: Possibilities and Challenges. *Adv. Mater.* **2012**, *24*, 229−251.
(22) Warren, S. C.; Thimsen, E. Plasmonic Solar Water Splitting. *Energy Environ. Sci.* **2012**, *5*, 5133−5146.

(23) Wu, K.; Rodríguez-Córdoba, W. E.; Yang, Y.; Lian, T. Plasmon-Induced Hot Electron Transfer from the Au Tip to CdS Rod in CdS-Au Nanoheterostructures. *Nano Lett.* **2013**, *13*, 5255−5263.
(24) Cushing, S. K.; Li, J.; Meng, F.; Senty, T. R.; Suri, S.; Zhi, M.; Li, M.; Bristow, A. D.; Wu, N. Photocatalytic Activity Enhanced by Plasmonic Resonant Energy Transfer from Metal to Semiconductor. *J. Am. Chem. Soc.* **2012**, *134*, 15033−15041.
(25) Thrall, E. S.; Steinberg, A. P.; Wu, X.; Brus, L. E. The Role of Photon Energy and Semiconductor Substrate in the Plasmon-Mediated Photooxidation of Citrate by Silver Nanoparticles. *J. Phys. Chem. C* **2013**, *117*, 26238−26247.
(26) Fowler, R. H. The Analysis of Photoelectric Sensitivity Curves for Clean Metals at Various Temperatures. *Phys. Rev.* **1931**, *38*, 45−56.
(27) Knight, M. W; Wang, Y.; Urban, A. S.; Sobhani, A.; Zheng, B. Y.; Nordlander, P.; Halas, N. J. Embedding Plasmonic Nanostructure Diodes Enhances Hot Electron Emission. *Nano Lett.* **2013**, *13*, 1687−1692.
(28) Scales, C.; Berini, P. Thin-Film Schottky Barrier Photodetector Models. *IEEE J. Quantum Electron.* **2010**, *46*, 633−643.
(29) Chen, Q. Y.; Bates, C. W., Jr. Geometrical Factors in Enhanced Photoyield from Small Metal Particle. *Phys. Rev. Lett.* **1986**, *57*, 2737−2740.
(30) White, T. P.; Catchpole, K. R. Plasmon-enhanced Internal Photoemission for Photovoltaics: Theoretical Efficiency Limits. *Appl. Phys. Lett.* **2012**, *101*, 073905 1−3.
(31) Zhu, S.; Lo, G. Q.; Kwong, D. L. Theoretical Investigation of Silicide Schottky Barrier Detector Integrated in Horizontal Metal-Insulator-Silicon-Insulator-Metal Nanoplasmonic Slot Waveguide. *Opt. Express* **2011**, *19*, 15843−15854.
(32) Atar, F. B.; Battal, E.; Aygun, L. E.; Daglar, B.; Bayindir, M.; Okyay, A. K. Plasmonically Enhanced Hot Electron Based Photovoltaic Device. *Opt. Express* **2013**, *21*, 7196−7201.
(33) Tamm, I.; Schubin, S. Zur Theorie des Photoeffektes an Metallen. *Z. Phys.* **1931**, *68*, 97−113.
(34) Brodsky, A. M.; Gurevich, Yu. Ya. Theory of External Photoeffect from the Surface of a Metal. *Soviet Phys. - JETP* **1968**, *27*, 114−121.
(35) Protsenko, I. E.; Uskov, A. V. Photoemission from Metal Nanoparticles. *Phys.−Usp.* **2012**, *55*, 508−518.
(36) Zhukovsky, S. V.; Babicheva, V. E.; Uskov, A. V.; Protsenko, I. E.; Lavrinenko, A. V. Enhanced Electron Photoemission by Collective Lattice Resonances in Plasmonic Nanoparticle-Array Photodetectors and Solar Cells. *Plasmonics* **2013**, DOI: 10.1007/s11468-013-9621-z.
(37) Kornbluth, M.; Nitzan, A.; Seideman, T. Light-Induced Electronic Non-equilibrium in Plasmonic Particles. *J. Chem. Phys.* **2013**, *138*, 174707 1−10.
(38) Govorov, A. O.; Zhang, H.; Gun'ko, Y. K. Theory of Photoinjection of Hot Plasmonic Carriers from Metal Nanostructures into Semiconductors and Surface Molecules. *J. Phys. Chem. C* **2013**, *117*, 16616−16631.
(39) Esteban, R.; Borisov, A. G.; Nordlander, P.; Aizpurua, J. Bridging Quantum and Classical Plasmonics with a Quantum-Corrected Model. *Nat. Commun.* **2012**, *3*, 825 1−8.
(40) Scholl, A. J.; Ai Leen Koh, A. L.; Dionne, J. A. Quantum plasmon resonances of individual metallic nanoparticles. *Nature* **2012**, *483*, 421−427.
(41) Townsend, E.; Bryant, G. W. Plasmonic Properties of Metallic Nanoparticles: The Effects of Size Quantization. *Nano Lett.* **2012**, *12*, 429−434.
(42) Kraus, W. A.; Schatz, G. C. Plasmon Resonance Broadening in Small Metal Particles. *J. Chem. Phys.* **1983**, *79*, 6130−6139.
(43) García de Abajo, F. J. Nonlocal Effects in the Plasmons of Strongly Interacting Nanoparticles, Dimers, and Waveguides. *J. Phys. Chem. C* **2008**, *112*, 17983−17987.
(44) Toscano, G.; Raza, S.; Yan, W.; Jeppesen, C.; Xiao, S.; Wubs, M.; Jauho, A.-P.; Bozhevolnyi, S. I.; Mortensen, N. A. Nonlocal response in plasmonic waveguiding with extreme light confinement. *Nanophotonics* **2013**, *2*, 161−166.
(45) Platzman, P. M.; Wolf, P. A. *Waves and Interactions in Solid State Plasma*; Academic Press: New York, NY, 1973.
(46) Mermin, N. D. Lindhard Dielectric Function in the Relaxation-Time Approximation. *Phys. Rev. B* **1970**, *1*, 2362−2363.
(47) Johnson, P. B.; Christy, R. W. Optical Constants of the Noble Metals. *Phys. Rev. B* **1972**, *6*, 4370−4379.
(48) Link, S.; El-Sayed, M. A. Spectral Properties and Relaxation Dynamics of Surface Plasmon Electronic Oscillations in Gold and Silver Nanodots and Nanorodes. *J. Phys. Chem. B* **1999**, *103*, 8410−8426.
(49) Hartland, G. V. Optical Studies of Dynamics in Noble Metal Nanostructures. *Chem. Rev.* **2011**, *111*, 3858−3887.
(50) Davies, J. H. *The Physics of Low-Dimensional Semiconductors*, 1st ed.; Cambridge University Press: Cambridge, England, 1998.
(51) The DDA code was taken from the open source at http://www.astro.princeton.edu/~draine/DDSCAT.html (accessed July 2013).
(52) Willets, K. A.; Van Duyne, R. P. Localized Surface Plasmon Resonance Spectroscopy and Sensing. *Annu. Rev. Phys. Chem.* **2007**, *58*, 267−297.
(53) Draine, B. T.; Flatau, P. J. Discrete-dipole Approximation for Scattering Calculations. *J. Opt. Soc. Am. A* **1994**, *11*, 1491−1499.
(54) Flatau, P. J.; Draine, B. T. Fast Near Field Calculations in the Discrete Dipole Approximation for Regular Rectilinear Grids. *Opt. Express* **2012**, *20*, 1247−1252.
(55) Draine, B. T.; Flatau, P. J. User Guide for the Discrete Dipole Approximation Code DDSCAT 7.3: http://arxiv.org/abs/1305.6497 (accessed December 2013).